ASSOCIAZIONE NAZIONALE ITALIANA DI INGEGNERIA SISMICA
ANIDIS
Italian National Association of Earthquake Engineering

XVIII CONVEGNO ANIDIS
L'ingegneria sismica in Italia
ASCOLI PICENO 2019
15-19 Settembre

A hysteretic model based on plastic and damage mechanisms for seismic analysis of inelastic structures

Fabio Mazza[a]
[a] *Dipartimento di Ingegneria Civile, Università della Calabria, 87036 Rende (Cosenza), Italy*

Keywords: Hysteretic model; plastic mechanism; damage mechanism; damage evolution; nonlinear monotonic and cyclic analysis; nonlinear dynamic analysis.

ABSTRACT
A versatile hysteretic model based on plastic and damage mechanisms is presented here for seismic analysis of inelastic structures, that could serve as a simple approach to describe a vast range of experimentally observed behaviours. To begin with, piecewise linearization of the initial backbone curve is carried out, each linear segment being defined by an in-parallel combination of elastic-perfectly plastic (EPP) and elastic-softening damage (ESD) mechanisms. Each pair of plastic and damage mechanisms is expressed as function of a damage index depending on a damage variable. The i-th damage mechanism is also expressed in terms of two additional parameters related to the points defining the piecewise linear approximation of the initial backbone curve. Then, simulation of structural components is used to exemplify the reproduction of the main typologies of hysteretic models with different types of degradation. Comparison with experimental results available in the literature is subsequently carried out to calibrate the proposed model, with reference to r.c. columns with low building standards. Finally, nonlinear seismic analysis of a single-degree-of-freedom system, equivalent to a four-storey r.c. framed structure designed with a former seismic code, is used to generate the capacity boundary curve starting from the initial backbone curve.

1 INTRODUCTION

Observation of structural damage and collapse in past earthquakes has underlined the need for a proper description of the nonlinear behaviour of buildings, especially in the case of high seismic loads and low building standards (FEMA P440A 2009). It can be noted a great deal of difference in the force-displacement relationship corresponding to the monotonic loading (i.e. the initial backbone curve) and the envelope of the hysteretic response (i.e. the cyclic envelope), as the latter may be heavily loading-history dependent. Therefore, it is essential to develop a suitable hysteretic model that incorporates degradation laws of stiffness and strength with increasing inelastic deformation and upon reversals of loading cycles. In detail, stiffness degrading behaviour can be grouped in three main categories: i) with the same unloading and reloading degrading stiffness, as a function of the peak inelastic displacement; ii) with constant unloading stiffness and degrading reloading stiffness; iii) with different degrading laws for the unloading and reloading stiffnesses. In addition, structural systems frequently show a combination of two types of strength degradation, related to the peak inelastic displacement, with regard to increasing loading cycles, and related to the amount of hysteretic energy dissipation, in the case of repeated cyclic displacement. In-cycle strength degradation may also occur, which correspond to a loss of strength coupled with a negative post-yield stiffness in a given cycle. Furthermore, pinching phenomenon produced by cracks is frequently observed, characterized by notable reductions in reloading stiffness followed by recovery when displacement is imposed in the opposite direction.

By means of the various types of hysteretic behaviour above described, a great number of polygonal and smoothed hysteretic models with different levels of complexity are employed. These models follow evolutionary rules based on the actual strain combined with non-degrading or degrading properties dependent on the damage level, being able to be classified in three main groups: i) non-evolutionary non-degrading, with elastic unloading and reloading branches (e.g. the

elastic perfectly-plastic and elastic-plastic, with hardening or softening, models); ii) evolutionary non-degrading, with reloading rules depending on the actual level of strain (e.g. Takeda et al., 1970, and Song and Pincheira, 2000, polygonal models and smoothed models like those of Bouc, 1967, Wen, 1976, Sivaselvan and Reinhorn, 2000, and Vaiana et al. 2018); iii) evolutionary degrading, characterized by unloading and reloading rules as function of the damage state (e.g. Park et al., 1987, Ibarra et al., 2003, and Do and Filippou, 2018, models).

The deterioration of the backbone curve and cyclic deterioration rate are generally controlled by a continuously evolving damage variable (ψ) and corresponding damage index (Ψ). First damage functionals have been those based on the kinematic ductility and hysteretic energy dissipation and their combinations (Cosenza et al. 1993; Bozorgnia and Bertero 2003). A damage variable controlled by hysteretic energy dissipation has been related to parameters representative of cyclic deterioration as well as deterioration of the backbone curve (Ruiz-Garcia and Miranda 2005). Afterwards, to account for the loading history, the concept of primary and follower load cycles has been applied to indexes based on the cumulative inelastic deformations (Krätzig et al. 1989) and hysteretic energy (Mehanny and Deierlein 2001). The cyclic deterioration rate can be also controlled by using an improved parameter related to the energy dissipation, where weights of the energy dissipation increment under positive or negative forces are introduced to differentiate the effect of deformations exceeding the previous maximum values from the effect of lower deformations than these maximum values (Do and Filippou 2018).

In the present work, a hysteretic model based on plastic and damage mechanisms is proposed for assessment of the nonlinear behaviour due to strength and stiffness degradation. The effects of the model parameters are highlighted with reference to some typologies of hysteretic laws. Then, the proposed model is calibrated by experimental results available in the literature, which utilize r.c. columns subjected to monotonic and cyclic displacement histories (Sezen 2002). Finally, nonlinear seismic analysis of a single-degree-of-freedom system, equivalent to a four-storey r.c. framed structure designed with a former seismic code, is used to highlight that a more realistic estimation of the deformation capacity can be obtained using the proposed hysteretic model.

2 PLASTIC-DAMAGE HYSTERETIC MODEL

The analytical formulation of the proposed combined plastic-damage (CPD) hysteretic model is summarized below, with the main focus on the elastic-perfectly plastic (EPP) and elastic-softening damage (ESD) mechanisms.

2.1 Plastic mechanisms

The initial backbone curve with monotonically decreasing stiffness and increasing displacement until reaching final zero stiffness is fitted with a four-segment approximation (Figure 1a), distinguishing positive and negative forces ($F^{\pm}$) and displacements ($d^{\pm}$). By using such piecewise linear fit and leaving aside damage (i.e. a damage index Ψ=0), it is possible to couple the i-th linear segment with the corresponding i-th plastic mechanism (Figure 1b) described by an elastic-perfectly plastic law expressed as:

$$F_{P,i}^{\pm}=K_{P,i}^{\pm}\cdot\left(d^{\pm}-d_{y,i-1}^{\pm}\right),\quad \left|d_{y,i-1}^{\pm}\right|<\left|d^{\pm}\right|\leq\left|d_{y,i}^{\pm}\right| \tag{1}$$

$$F_{P,i}^{\pm}=F_{yP,i}^{\pm}=K_{P,i}^{\pm}\cdot\left(d_{y,i}^{\pm}-d_{y,i-1}^{\pm}\right),\quad \left|d^{\pm}\right|>\left|d_{y,i}^{\pm}\right| \tag{2}$$

$F_{yP,i}$ and $d_{y,i}$ being the force and displacement at the i-th yielding point and $K_{P,i}$ the elastic stiffness.

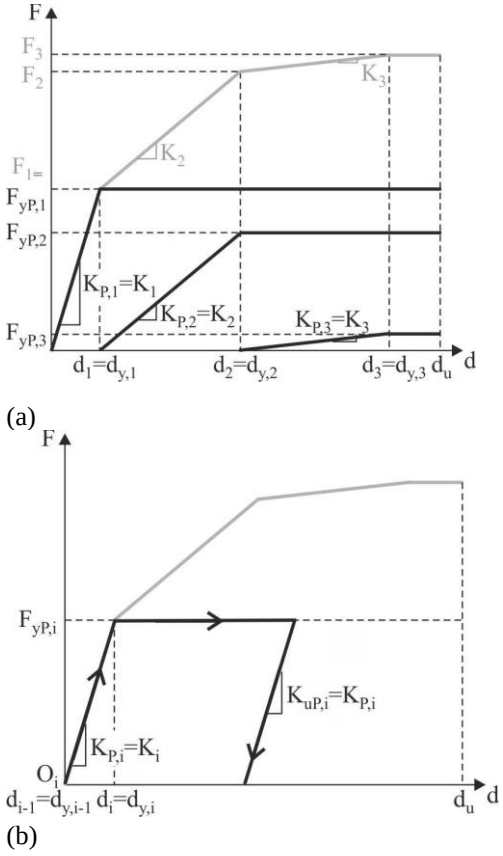

Figure 1. Illustration of the proposed hysteretic model with plastic mechanisms without damage (Ψ=0) for monotonic (a) and i-th cyclic (b) EPP mechanisms.

Deterioration in strength and stiffness is not modelled and the unloading stiffness of the i-th plastic mechanism is as the elastic one. Note that the reloading stiffness resulting from the combination of N plastic mechanisms is less than or equal to the unloading one.

A second shape of the initial backbone curve is that exhibiting multi-linear elastic hardening with a final positive-stiffness segment. In this case, the last (i.e. N-th) plastic mechanism of the hysteretic model will be represented by an elastic-linear law. Moreover, the proposed model is also able to describe cases involving quadrilinear elastic-hardening-negative residual laws, with negative stiffness and low-strength zero-stiffness segment, respectively, by using a negative N-th elastic-perfectly plastic law.

2.2 Plastic and damage mechanisms

The proposed hysteretic model incorporates deterioration in stiffness and strength for loading cycles of increasing amplitude. Moreover, the cyclic deterioration is explicitly incorporated in the model by modifying the initial backbone curve, representative of the response for monotonically increasing loading, as function of the cyclic loading history. To ensure this result, the overall hysteretic behaviour is evaluated through the overlapping of N plastic (Figure 2a) plus N damage mechanisms (Figure 2b), where N corresponds exactly to the number of segments of the piecewise linear fit of the initial backbone curve. Specifically, the i-th damage mechanism presents an elastic-softening law characterized by a first linear upward branch until the attainment of yield displacement of the corresponding i-th plastic mechanism

$$F_{D,i}^{\pm}=K_{D,i}^{\pm}\cdot\left(d^{\pm}-d_{y,i-1}^{\pm}\right),\quad \left|d_{y,i-1}^{\pm}\right|<\left|d^{\pm}\right|\leq\left|d_{y,i}^{\pm}\right| \tag{3}$$

with an elastic stiffness

$$K_{D,i}^{\pm}=\Psi^{\pm}\cdot K_i^{\pm} \tag{4}$$

Ψ being a damage index function of a damage variable ψ.

Since the stiffness of the i-th segment of the backbone curve results from an in parallel combination of plastic (Figure 3a) and damage (Figure 3b) mechanisms

$$K_i^{\pm}=K_{P,i}^{\pm}+K_{D,i}^{\pm} \tag{5}$$

the initial plastic stiffness can be written as

$$K_{P,i}^{\pm}=\left(1-\Psi^{\pm}\right)\cdot K_i^{\pm} \tag{6}$$

with damage index Ψ allowing for a separation between positive (Ψ^{+}) and negative (Ψ^{-}) effects. At each step of the loading history, the unknown stiffnesses of the plastic (i.e. $K_{P,i}$, i=1,..,N) and damage (i.e. $K_{D,i}$, i=1,..,N) mechanisms need to be updated, on the basis of the current level of damage defined by parameter Ψ, by means of Equations (4) and (6). It should be noted that the i-th pair of plastic and damage mechanisms is able to reproduce the degradation of stiffness of the corresponding segment of the initial backbone curve. In fact, the fourth zero stiffness segment of the backbone curve shown in Figures 3a,b is not reproduced when a value of Ψ>0 is considered. Moreover, the proposed hysteretic model allows for the reproduction of a softening segment and/or a residual plateau of the force-displacement law through a final negative coupling of plastic and damage mechanisms. Finally, pinching effect can be reproduced modifying the unloading/reloading branch of the i-th cyclic ESD mechanism.

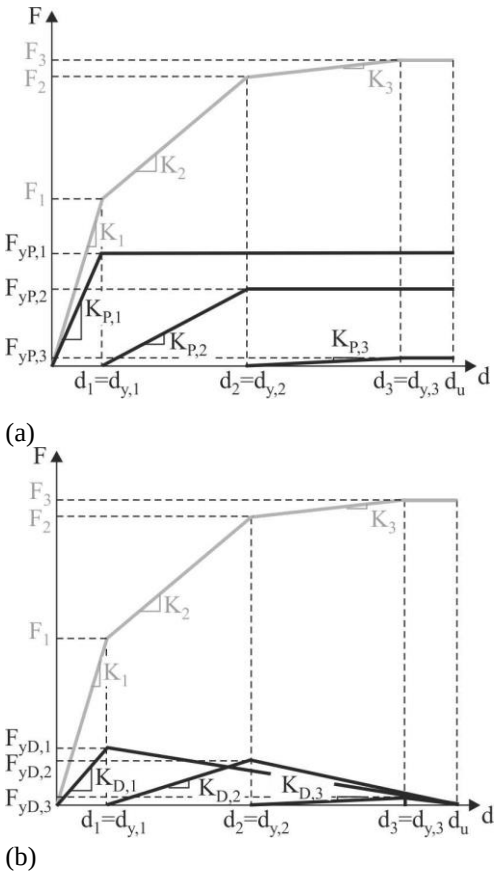

Figure 2. Main cases for the proposed hysteretic model with plastic and damage mechanisms (0<Ψ<1): monotonic EPP (a) and ESD (b) mechanisms for a backbone curve with hardening.

Thereafter, the second linear downward branch of the i-th monotonic elastic-softening damage (ESD) mechanism comes out of the expression (Figure 3b)

$$F_{D,i}^{\pm}=F_{yD,i}^{\pm}-K_{sD,i}^{\pm}\cdot\left(d^{\pm}-d_{y,i}^{\pm}\right),\quad \left|d_{y,i}^{\pm}\right|<\left|d^{\pm}\right|\leq\left|d_{u}^{\pm}\right| \tag{7}$$

where the stiffness of the softening branch is

equal to

$$K_{sD,i}^{\pm}=\alpha_i^{\pm}\cdot K_{D,i}^{\pm}=\alpha_i^{\pm}\cdot\Psi^{\pm}\cdot K_i^{\pm}=\alpha_i^{\pm}\cdot\frac{\Psi^{\pm}}{1-\Psi^{\pm}}\cdot K_{P,i}^{\pm} \quad (8)$$

being

$$\alpha_i^{\pm}=\left(d_{y,i}^{\pm}-d_{y,i-1}^{\pm}\right)\Big/\left(d_u^{\pm}-d_{y,i}^{\pm}\right) \quad (9)$$

where d_u is the displacement at the ultimate point of the initial backbone curve. A strength decay of the latter is initially introduced by parameter α_i, whose value is generally different for each ESD mechanism, and its cyclic deterioration is subsequently controlled by damage index Ψ.

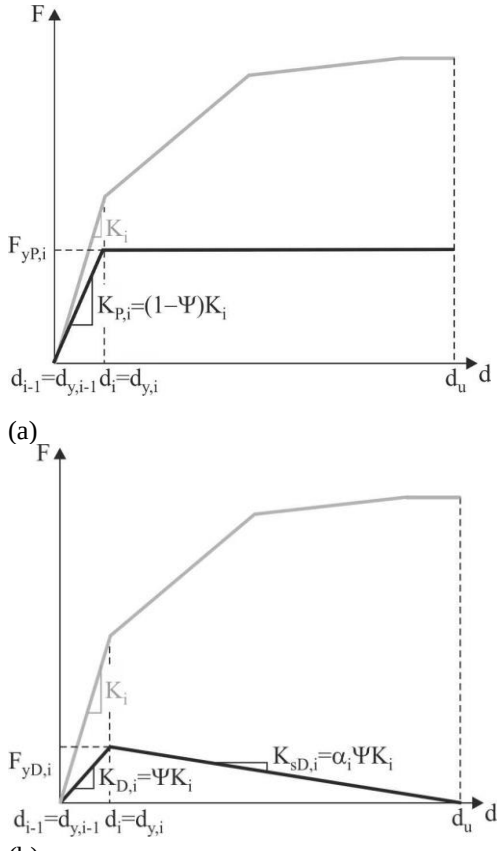

Figure 3. Illustration of the proposed hysteretic model with plastic and damage mechanisms ($0<\Psi<1$): (a) i-th monotonic EPP (a) and ESD (b) mechanisms.

It should be noted that the combination of α_i and Ψ also allows the reproduction of cyclic (i.e. strength loss occurring in cycles subsequent to the current loading cycle) and in-cycle (i.e. strength loss occurring during the loading cycle) degradation. Finally, the unloading stiffness of the i-th cyclic EPP) mechanism is assumed equal to that of the loading branch (Figure 4a), while the elastic-softening damage (ESD) mechanism is characterized by:

$$K_{uD,i}^{\pm}=\beta_i^{\pm}\cdot K_{D,i}=\beta_i^{\pm}\cdot\Psi^{\pm}\cdot K_i^{\pm}=\beta_i^{\pm}\cdot\frac{\Psi^{\pm}}{1-\Psi^{\pm}}\cdot K_{P,i}^{\pm} \quad (10)$$

given

$$\beta_i^{\pm}=\alpha_i^{\pm}\cdot\left(d_u^{\pm}-d_i'^{\pm}\right)\Big/\bar{d}_i^{\pm} \quad (11)$$

where d' is the displacement corresponding to the initial point of the unloading phase that is part of the softening branch (Figure 4b). In so doing, the unloading branch of the i-th ESD mechanism is oriented towards the origin. Moreover, the unloading and reloading stiffness reductions are governed by parameter β_i, which is expressed as function of α_i, while their cyclic deterioration here again depend on damage index Ψ. As can be observed, the parameter α_i (i=1,..,N) is function of the points defining the piecewise linear approximation of the initial backbone curve, taking a different value for each ESD mechanism, while parameter β_i (i=1,..,N) depends on parameter α_i and displacement corresponding to the initial point of the unloading phase.

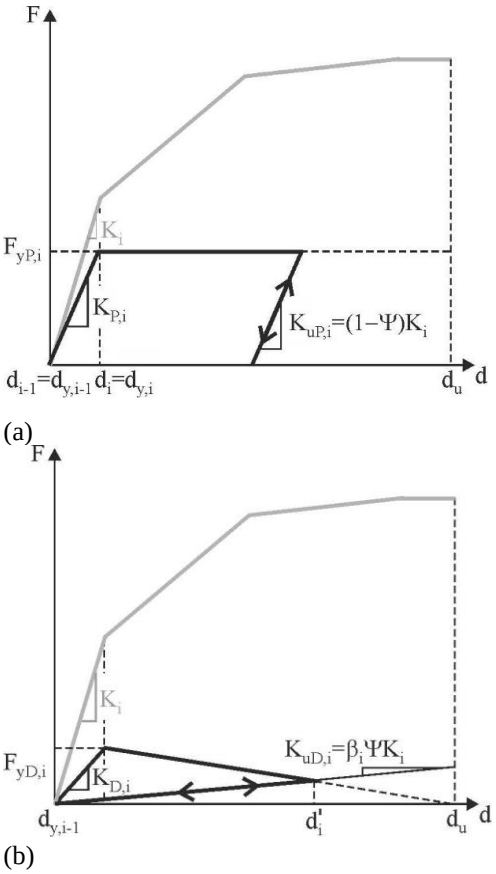

Figure 4. Illustration of the proposed hysteretic model with plastic and damage mechanisms ($0<\Psi<1$): (a) i-th cyclic EPP (a) and ESD (b) mechanisms.

A simplified function is chosen to represent the damage growth, which is only a first step, although theoretically sound damage parameters are available in literature and could be implemented within the framework of the proposed model (Do and Filippou 2018). In particular the cyclic deterioration of the plastic and damage mechanisms described above is controlled by a damage index Ψ, which involves a damage variable ψ representing the inelastic deformation, varying between Ψ=0, when there is

no damage, and Ψ=1, when failure occurs (Kappos 1997). The lower bound threshold of damage variable ψ (i.e. ψ_e) corresponds to a substantially linear elastic response, highlighting threshold below which no damage occurs. Moreover, the upper bound threshold (i.e. ψ_u) represents the value of ψ at which failure occurs, corresponding to part or all of the ultimate capacity of the system under monotonically increasing load (i.e. ψ_{mon}). The shape of the ever-increasing Ψ-ψ law is

$$\Psi^{\pm}=0, \text{ for } \psi^{\pm}\leq\psi_e^{\pm} \quad (12a)$$

$$\Psi^{\pm}=\left(\frac{\psi^{\pm}-\psi_e^{\pm}}{\psi_u^{\pm}-\psi_e^{\pm}}\right)^{\varepsilon} \text{ for } \psi^{\pm}>\psi_e^{\pm},\ \varepsilon>0 \quad (12b)$$

ψ being the current value of the damage variable by nonlinear seismic analysis and ε an additional degradation rate parameter. Further details can be found in a previous work (Mazza 2019).

3 DAMAGE EVOLUTION IN THE PLASTIC-DAMAGE MODEL

In order to assess the effects of the damage index variability on the strength and stiffness degradation of the CPD model, a sensitivity analysis is carried out considering constant values of Ψ selected in the range [0-1[. In detail force-displacement laws obtained by overlapping the elastic perfectly-plastic (i.e. $F^{(EPP)}$ and $d^{(EPP)}$ in Figures 5a-7a) and elastic-softening damage (i.e. $F^{(ESD)}$ and $d^{(ESD)}$ in Figures 5b-7b) mechanisms are compared with their combined response (i.e. $F^{(CPD)}$ and $d^{(CPD)}$ in Figures 5c-7c). A multilinear (initial) backbone curve is also added (see red line) to the CPD mechanisms, whose main points define the α_i and β_i parameters of each pair of plastic and damage mechanisms (see Equations 9 and 11). Indeed, a few of cycles are reproduced in Figures 5-7, on the assumption that $d_{max}<d_u$. Moreover, all curves are normalized with reference to ultimate values of force (i.e. $F_u^{(CPD)}$) and displacement (i.e. $d_u^{(CPD)}$) of the combined plastic-damage mechanisms. As can be observed, the hysteretic energy dissipation of the EPP mechanisms declines for increasing values of Ψ, while the opposite is the case for the ESD mechanisms. The limit values Ψ=0 (Figure 5) and Ψ=0.99 (Figure 7) correspond to zero contribution of the ESD and EPP mechanisms, respectively. The $F^{(CPD)}$-$d^{(CPD)}$ curve always has a peak oriented stiffness degradation at reloading, pointing to the maximum inelastic displacement in the loading direction when taking Ψ>0, and an origin-oriented response for high values of Ψ.

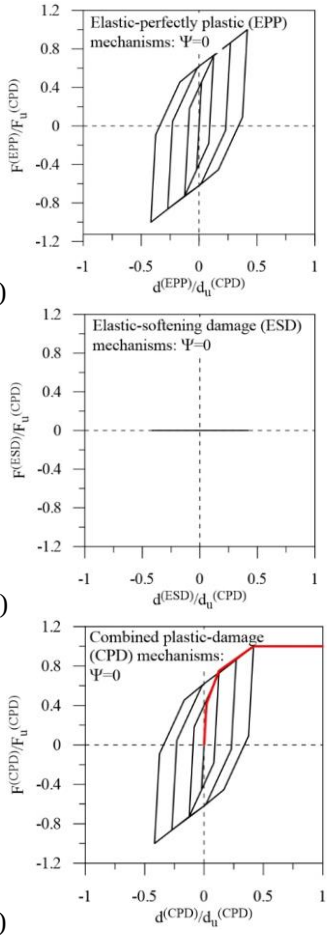

Figure 5. Hysteretic models for the damage index Ψ=0.

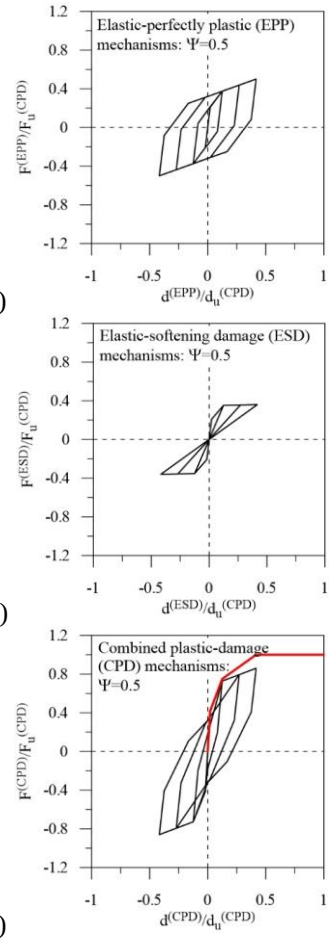

Figure 6. Hysteretic models for the damage index Ψ=0.5.

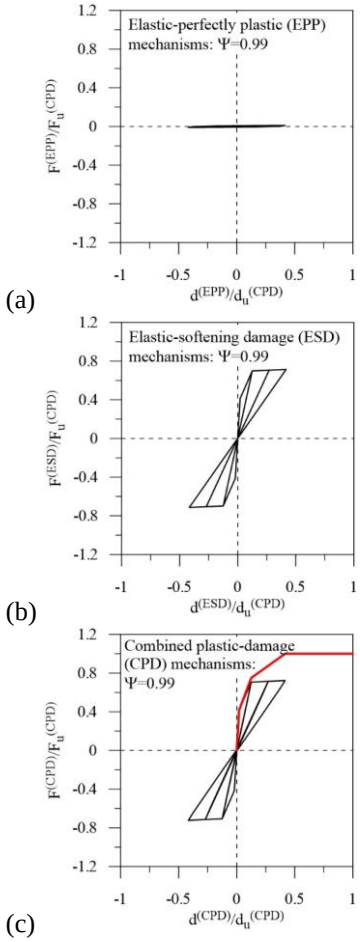

Figure 7. Hysteretic models for the damage index Ψ=0.99.

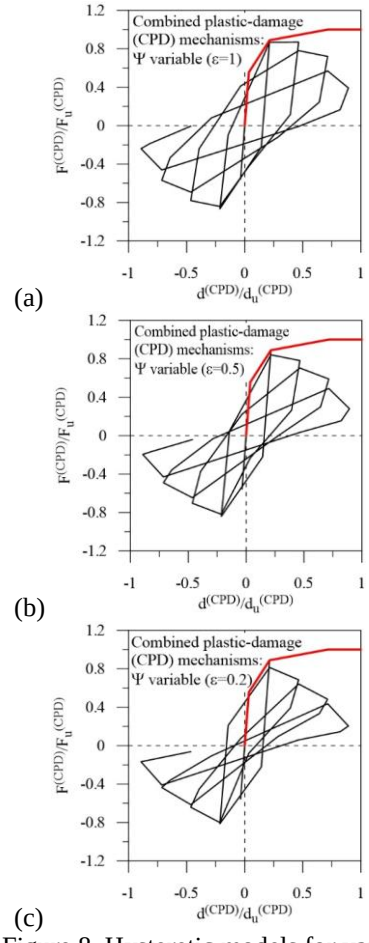

Figure 8. Hysteretic models for variable damage index *Y*.

A good fit between low values of Ψ and hysteretic response is obtained, highlighting a ductile behaviour characterized by full hysteresis loops and considerable energy dissipation for $\Psi \leq 0.5$ (Figures 5 and 6). On the other hand, brittle behaviour with moderate to severe pinching effects during the reloading phase corresponds to cases where $\Psi > 0.5$ (Figure 7). The force-displacement plastic-damage cyclic envelope moves inward as a result of cyclic degradation, leading to a decrease in strength and stiffness as a function of Ψ. Note that pinching effects are governed by the ESD mechanisms of the proposed model, which are in turn dependent on the cyclic reversed loading of structural components subjected to cyclic reversals

Effects of different evolution laws of damage on the CPD model are shown in Figure 8, where varying values of the damage index (Ψ) are assumed (Equations 12a,b), as a function of a damage variable the same as the imposed displacement (i.e. $\psi = d$). In order to reveal how much the damage index depends on the contribution of maximum inelastic deformation and energy dissipation, three values are considered for the exponent ε representing the rate of degradation: i.e. ε=1 (Figure 8a), ε=0.5 (Figure 8b) and ε=0.2 (Figure 8c).

Let us begin by saying that the increase of damage index Ψ for decreasing values of exponent ε is more likely to occur when the damage variable $\psi \leq 0.5\,\psi_u$ is assumed, while less notable changes of Ψ are observed when $\psi \rightarrow \psi_u$. Significant differences in the unloading and reloading stiffnesses are found when comparing the cyclic responses obtained with ε=1 (Figure 8a) and ε<1 (Figures 8b,c). The hysteretic energy dissipation corresponding to ε=0.5 and ε=0.2 (i.e. poorly equipped structural members) is comparable and lower than in the case of ε=1. A sudden reduction in strength is also observed for low values of ε (e.g. ε=0.2). Cyclic degradation effects characterized by loss of strength as well as stiffness occur in subsequent cycles. This result highlights that a variable damage index Ψ instead of a simplified constant value is required for an accurate description of cyclic degradation.

4 TEST STRUCTURES AND LOADING PROTOCOLS

First, two full scale r.c. columns shown in Figure 9a, representative of frame members of existing buildings designed in line with a former building code, are considered as test structures for the experimental calibration of the proposed CPD

hysteretic model. In particular, these specimens have square cross-sections and include heavily reinforced top and bottom beams, which simulate a rigid foundation and a rigid floor slab (Sezen 2002). A longitudinal steel reinforcement ratio of 2.5% is considered, assuming that the average yield and ultimate strengths of the longitudinal bars are 438 MPa and 645 MPa, respectively. An uniform spacing of the transversal ties is assumed, with measured yield and ultimate strengths equal to 476 MPa and 724 MPa, respectively Moreover, the average concrete cylindrical strength is about 21 MPa. Both specimens are subjected to a constant axial load of 667 kN, but have different cyclic lateral displacement histories.

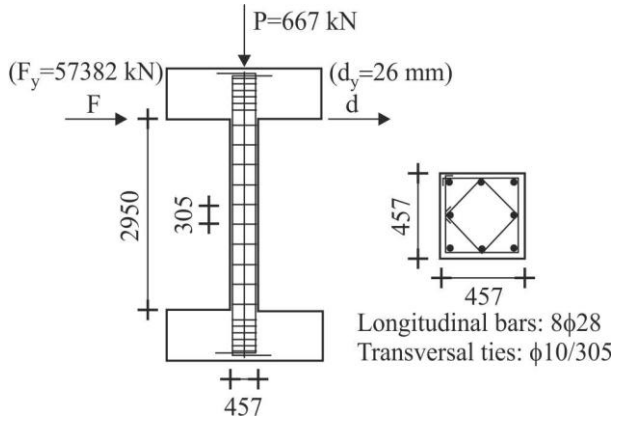

(a) Longitudinal and transversal sections.

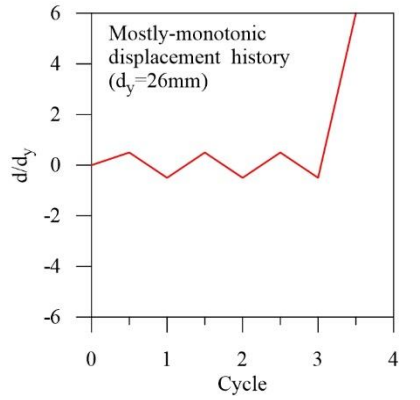

(b) Experimental loading protocol n.1.

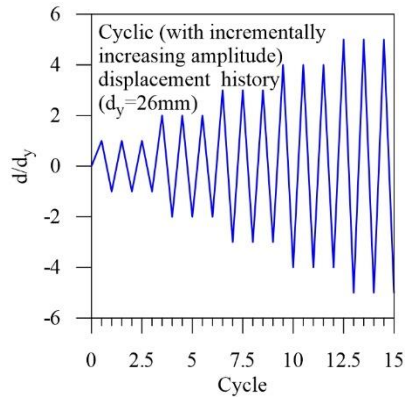

(c) Experimental loading protocol n.2.

Figure 9. First test structure (units in mm).

Specifically, the first specimen (corresponding to column n.4 of the experimental program) is subjected to a mostly monotonic protocol, characterized by cyclic displacements before the yield value (d_y=26 mm) followed by a monotonically increasing lateral displacement until failure is reached (Figure 9b). On the other hand, a cyclic protocol is considered for the second specimen (corresponding to column n. 1 of the experimental program) consisting in the application of three cycles of a fraction of the nominal yield value (d_y), followed by sequences of displacement cycles increased incrementally (i.e. three cycles of d_y, $2d_y$, $3d_y$, etc.) until failure occurs (Figure 9c).

Afterwards, a four-storey r.c. framed building of regular 3m interstorey height and 5m long bays and symmetric plan (Figure 10), is considered as test structure for the numerical (nonlinear static and dynamic) investigation.

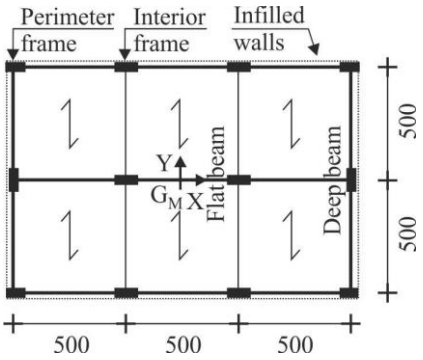

(a) Plan.

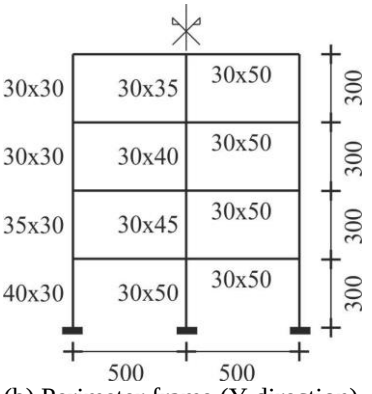

(b) Perimeter frame (Y direction).

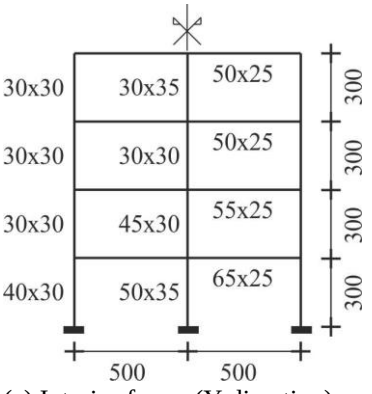

(c) Interior frame (Y direction).

Figure 10. Second test structure (units in cm).

The plane frames, whose geometric dimensions are shown in Figures 10b,c, represent the seismic behaviour of the building in the weakest direction (i.e. Y direction in Figure 10a) where flat beams in the interior frames are parallel to the direction of the floor slab. A simulated design of the framed building is carried out in accordance with a former Italian code (D.M. 1996), for medium-risk seismic region (seismic coefficient: C=0.07) and typical subsoil class (main coefficients: R=ε=β=1). The gravity loads are represented by a live load of 1.5 kN/m^2 on the top floor and 2.0 kN/m^2 on the other floors, and a dead load of 5.0 kN/m^2 on all the floors; an average weight of about 1.9 kN/m^2 is considered for the masonry infill walls. Concrete cylindrical compressive strength of 25 MPa and steel reinforcement with yield strength of 375 MPa are also considered. The design complies with the ultimate and serviceability limit states, satisfying minimum percentages of longitudinal bars for the r.c. frame members. The fundamental vibration period of the test structure along Y is equal to 0.71s, while the corresponding effective mass is equal to 82% of the total mass of the building. Further details on the design of the test structure can be found in a previous paper by the author (Mazza 2018). Seven recorded ground motions, reflecting the provisions of the Italian seismic code (N.T.C. 2018) for the geographical coordinates at the site in question (i.e. subsoil class B), are taken from the European Strong Motion database (Luzi et al. 2016) and scaled to match, on average, the design spectrum. The main data are reported in Table 1: i.e. earthquake, identification number (ID); magnitude (M_w), peak ground acceleration in the horizontal direction (PGA_H) and corresponding scale factor (SF_H).

Table 1. Main data of the selected earthquakes.

Earthquake	ID	M_w	PGA_H	SF_H
Friuli (aftershock)	65	6.0	0.336g	0.884
Montenegro	93	6.9	0.363g	0.819
Campano Lucano	146	6.9	0.176g	1.690
Kalamata	192	5.9	0.297g	1.002
Kalamata	192	5.9	0.240g	1.238
Erzincan	250	6.6	0.513g	0.580
South Iceland	1635	6.5	0.512g	0.582

5 NUMERICAL RESULTS

The proposed plastic-damage hysteretic model is first implemented in a homemade computer code for the pseudo-static (monotonic and cyclic) nonlinear analysis (Mazza and Mazza 2010), A set of EPP and ESD mechanisms is chosen to represent the piecewise fit of the initial backbone curve obtained by monotonic loading of the test structure. Before the numerical (cyclic) analysis, a piecewise linear approximation of the force-displacement backbone curve of the first test structure, based on the experimental curve (see red line in Figure 11) corresponding to the mainly monotonic loading protocol (Figure 9b), is built. Note that six parameters are involved in the trilinear backbone curve, capturing yield (i.e. point P_1), peak (i.e. point P_2) and residual (i.e. point P_3=P_u) strengths. Consequently, three pairs of EPP and ESD mechanisms are evaluated, where parameters of the i-th pair (i.e. α_i and β_i represented by Equations 9 and 11, respectively) are expressed in terms of the displacements (i.e. d_{yi} and d_u) defining the characteristic points of the trilinear backbone curve. It is worth noting that the contribution of the ESD mechanisms depends on the current value of the selected (constant or variable) damage index Ψ. Moreover, three parameters are needed to describe the evolution of damage index Ψ (see Equations 12a,b), two of which are already known (i.e. ψ_e=d_y and ψ_u=d_u), while the third (i.e. ε) is required to provide satisfactory matching between the experimental and analytical results. A step-by-step procedure is subsequently adopted, allowing continuous reproduction of the deteriorating hysteretic behaviour. At each step of the analysis, the algorithm computes the current value of the damage index and modifies loading and unloading stiffnesses of the plastic and damage mechanisms accordingly.

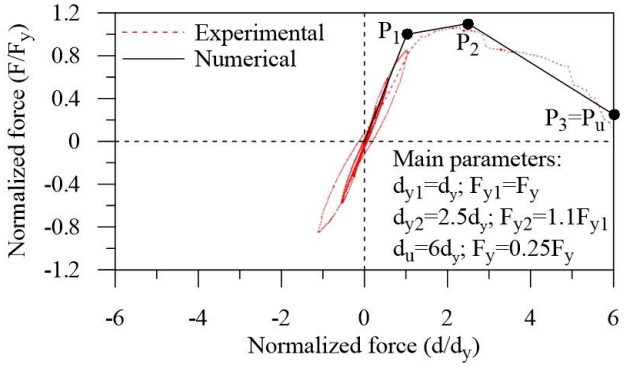

Figure 11. Pushover capacity curve and piecewise linear fit for cyclic analysis of the first test structure.

Then, a full-scale experimental test on r.c. columns from the literature (Sezen 2002) is used to calibrate the CPD model and verify its ability to reproduce inelastic cycles, vis-à-vis constant axial load and the cyclic loading protocol shown in Figure 9c. Experimental force-displacement curves (solid red lines) are plotted in Figures 12 and 13, with regard to a stepwise increasing loading history, while numerical results (solid

black lines) are represented in terms of a force-displacement law of an SDOF system equivalent to the structure shown in Figure 9a. In particular, results for low (Ψ=0.33), medium (Ψ=0.5) and high (Ψ=0.83) constant values of the damage index (Figure 12) are compared with the hysteretic response obtained on the basis of the calculation of a continuous damage evolution (Figure 13) with linear (ε=1.0) and nonlinear (ε=0.5 and ε=0.2) laws related to the parameter governing the rate of degradation.

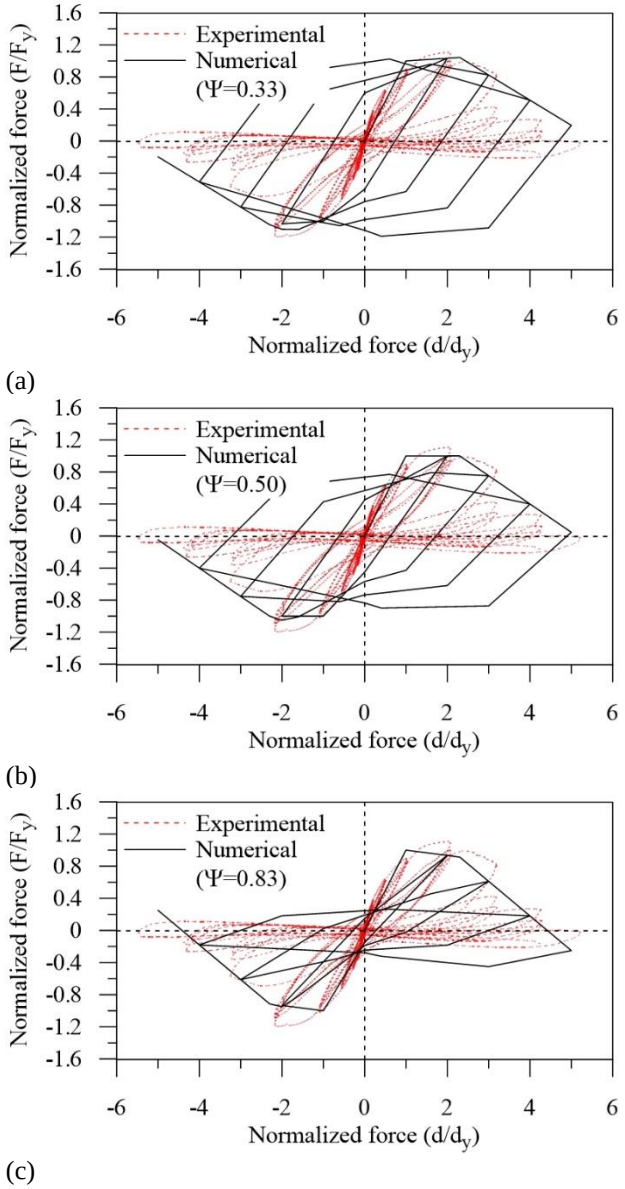

Figure 12 Comparison between numerical (with constant values of the damage index) and experimental results.

The proposed CPD model provides a reasonable assessment of the experimental (monotonic) curve enveloping the hysteretic response when a high (constant) value of damage index Ψ (Figure 12c) or damage variability depending on the current value of the inelastic deformation (Figure 13) are considered. An acceptable fit with the experimental cyclic response is partially guaranteed only during the unloading phases for an updating value of Ψ, in line with nonlinear degradation rules (Figures 13b,c). Pinching phenomena cannot be adequately controlled in the basic formulation of the ESD mechanisms governed by Equations (9) and (11). Moreover, it should be noted that the unloading and reloading phases occur along the same straight line resulting from a damage index as function of the maximum inelastic displacement, independently of cumulative inelastic deformations and dissipated energy. It is not possible, therefore, to capture the internal cycles of the *F-d* experimental laws when three cycles are applied for each peak displacement, in line with the second loading protocol (Figure 9c). Nevertheless, such straight lines appropriately reproduce the global hysteretic response, capturing the key values (i.e. minimum and maximum) of the cyclic displacements.

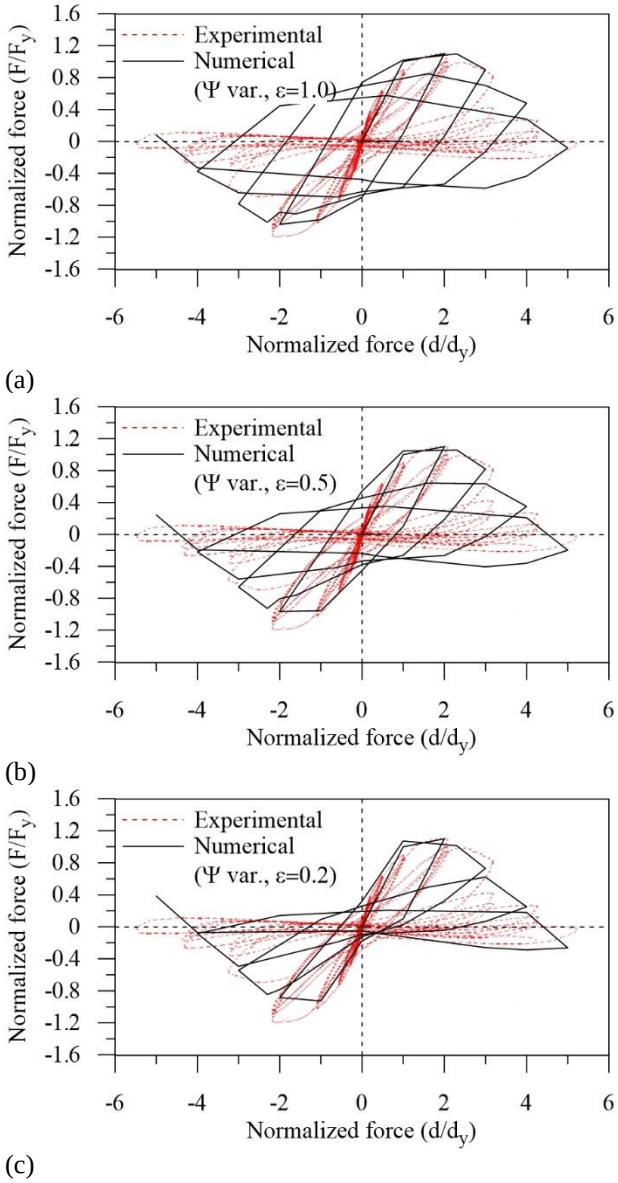

Figure 13 Comparison between numerical (with variable values of the damage index) and experimental results.

It is worth noting that the selection of a more sophisticated damage index based on combination of the hysteretic energy and inelastic deformation, given the combination of plastic and damage mechanisms, would make it possible to better reproduce experimental loops of degrading systems. From this point of view, the proposed CPD model should be considered as work in progress, until an appropriate damage index is calibrated.

Numerical studies confirm that it may possible to estimate the complex effects of strength and stiffness degradation on seismic response of a multi-degree-of-freedom (MDOF) system through the nonlinear dynamic analysis of an equivalent SDOF system (Vamvatsikos and Cornell 2005). Specifically, nonlinear static analysis is used to generate an idealized force-deformation curve of the MDOF system, which is then used as a force-displacement capacity boundary to constrain the hysteretic behaviour. In this way, a piecewise linear fit of the pushover curve can be used as the initial backbone curve when applying the CPD model to the equivalent nonlinear SDOF system. To illustrate this procedure, the CPD model is applied to the nonlinear SDOF system equivalent to the second test structure shown in Figure 10. A nonlinear static (pushover) analysis of the framed structure along the Y direction is carried out, under constant gravity loads and monotonically increasing horizontal loads. A "modal" lateral-load pattern is adopted, proportional to the first mode (horizontal) components multiplied by the corresponding floor masses. A step-by-step procedure based on the arc-length iteration scheme is adopted in the pushover analysis (Mazza 2018), assuming a value r_F=1% for the hardening ratio of the r.c. frame members. Capacity curves of the MDOF system and equivalent SDOF system that mimics its nonlinear behaviour are shown in Figure 14, considering the base shear (F_{base}) and the horizontal top displacement (d_{top}).

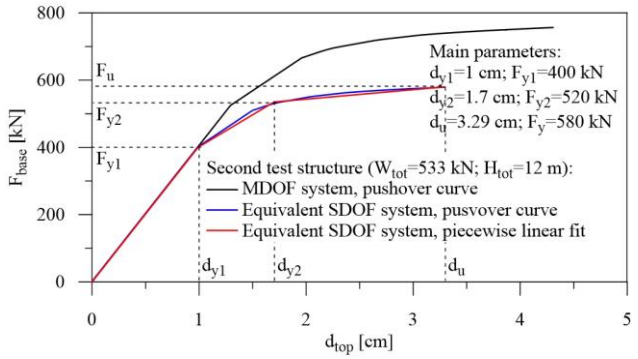

Figure 14. Pushover capacity curve and piecewise linear fit for cyclic analysis of the second test structure.

The total seismic weight of the structure (W_{tot}) and the building height (H_{tot}) are also reported as a reference. Note that the ultimate value of displacement corresponds to the ultimate value of curvature ductility demand at critical sections of the r.c. frame members, evaluated in accordance with the provisions of the Italian seismic code for existing buildings (N.T.C. 2018). The capacity curve of the original structure is converted into the pushover curve of an equivalent SDOF system, computing reduced forces and displacements based on the first mode participation factor of the MDOF system along the Y direction (i.e. Γ_Y=1.31).

Then, an implicit two-parameter integration scheme and an initial stress like iterative procedure are used for the nonlinear dynamic analysis of the second test structure subjected to horizontal ground motion (Mazza and Mazza, 2010). Nonlinear time-history analyses of the SDOF system are carried out, considering seven ground motions matching, on average, the life-safety (LS) acceleration design spectrum of the original building. Specifically, force-displacement curves resulting from the CPD model are plotted in Figures 15 and 16, with reference to constant values of the damage index (i.e. Ψ=0.33, 0.5 and 0.83 in Figures 15a,b,c, respectively) and variable values of Ψ depending on peak inelastic deformation (i.e. assuming rate degradation of damage governed by ε=1, 0.5 and 0.2 in Figures 16a,b,c respectively). As shown, the main modes of cyclic deterioration induced by each ground motion are highly sensitive to the damage process during the loading history, stressing the importance of having a computationally efficient and numerically accurate structural model able to describe the softening behaviour of structural components, especially under extreme loading conditions. In particular, stiffness reduction upon unloading and reloading are already apparent for low-to-medium (constant) values of Ψ (Figures 15a,b), while strength decay related to pinching effects and cyclic and in-cycle degradations only appears for high values of Ψ (Figure 15c) and continuous linear (Figure 16a) and nonlinear (Figures 16b,c) damage evolution. It should be noted that similar curves are obtained for different ground motions when constant values of the damage index are considered (Figure 15), since these curves have only one capacity boundary curve in common. On the other hand, some slight differences are observed in the case of a variable damage index (Figure 16) given that selected records are scaled to match the (elastic) design response spectrum of acceleration.

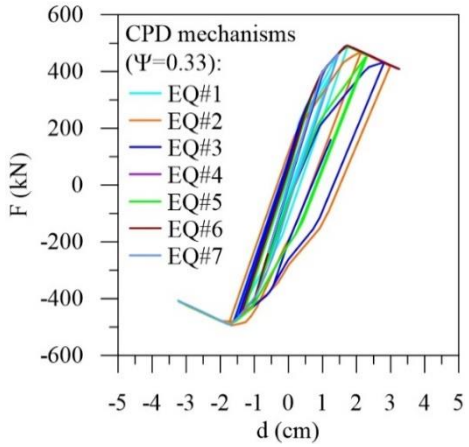

(a)

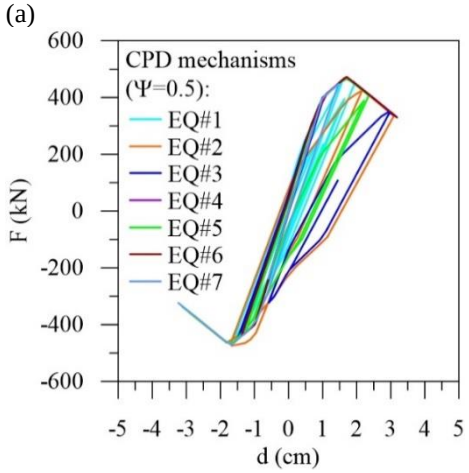

(b)

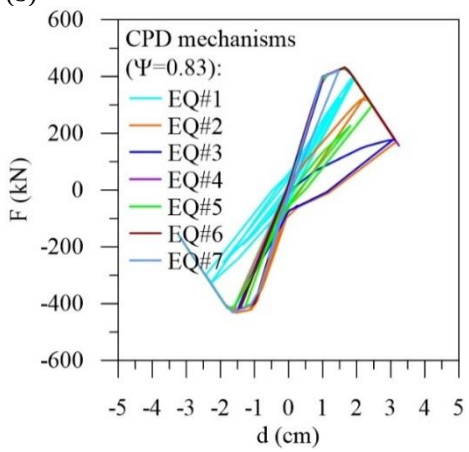

(c)

Figure 15. Cyclic response (constant values of the damage index) of the nonlinear SDOF equivalent to the second test structure, subjected to selected earthquakes matching life-safety design spectrum.

Finally, the force-displacement curves that envelope the hysteretic response of the equivalent SDOF system (i.e. the cyclic envelopes) are plotted in Figure 17, together with the monotonic trilinear curve resulting from nonlinear static analysis of the second test structure. In detail, the cyclic envelopes correspond to constant (Figure 17a) and variable (Figure 17b) values of damage index Ψ and are formed as an average of those separately obtained for each of the seven accelerograms.

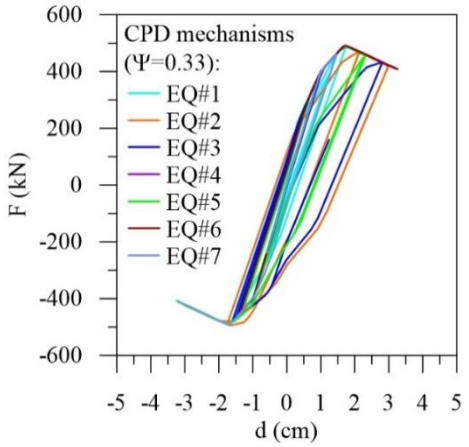

(a)

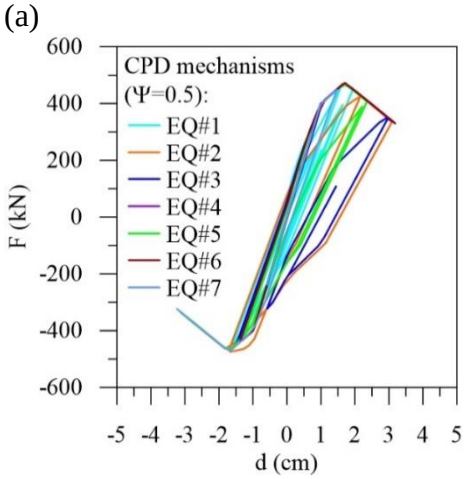

(b)

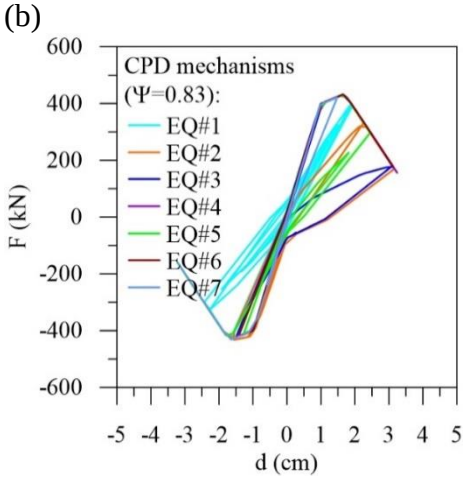

(c)

Figure 16. Cyclic response (variable values of the damage index) of the nonlinear SDOF equivalent to the second test structure, subjected to selected earthquakes matching life-safety design spectrum.

It is interesting to note that the capacity boundary curves are strongly influenced by the dynamic nature of the loading protocol and the stiffness and strength deteriorating rules of the CPD model, which are in some cases smaller and in others significantly smaller than the capacity boundary curve for monotonic loads. This confirms once again the importance of accounting for the nonlinear cyclic response accurately, also because performance-based design procedures are frequently based on monotonic (pushover) force-

displacement curves that do not include information on the hysteretic behaviour of the structural system.

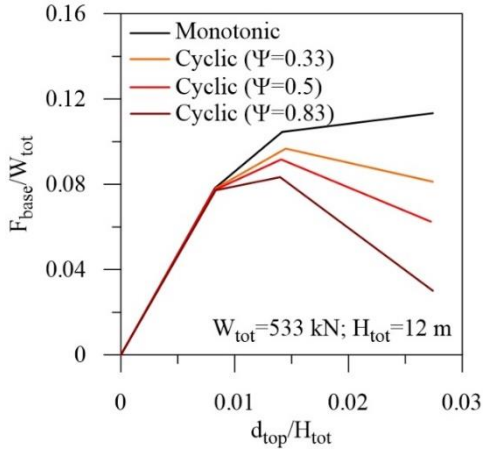

(a)

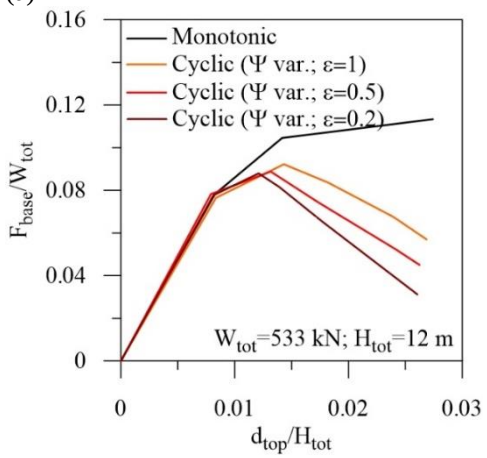

(b)

Figure 17. Capacity boundary curve for the nonlinear SDOF equivalent to the second test structure subjected to selected earthquakes matching life-safety design spectrum.

6 CONCLUSIONS

A hysteretic model based on combined plastic and damage mechanisms (CPD model), deriving from the assumption that the nonlinear monotonic response is known, is first developed and then implemented in a C++ computer code for the nonlinear static (cyclic) and dynamic (seismic) analysis. An in-parallel combination of EPP and ESD mechanisms is obtained through a piecewise linear fit of the initial backbone curve.

The effects of different damage levels on the CPD model are firstly investigated by considering constant values of the damage index. As expected, the hysteretic energy dissipation of the EPP mechanisms declines for increasing values of Ψ, while the opposite happens for the ESD mechanisms. A good correlation is shown between low values of Ψ and ductile behaviour, characterized by hysteretic loops with large energy dissipation capacity, and high values of Ψ and brittle behaviour, with moderate to severe pinching during the reloading phase. Then, effects of different damage evolution laws are also analysed with reference to linear (ε=1) and nonlinear (ε<1) degradation rules of the damage index. It is resulted that the hysteretic energy dissipation corresponding to ε<1 is lower than that corresponding to ε=1, reflecting structural members with poor detailing.

The proposed CPD model is validated against full-scale experimental tests on r.c. columns subjected to constant axial load and mostly monotonic and stepwise increasing horizontal loads. In particular, the results for low, medium and high constant values of the damage index are compared with those obtained on the basis of a continuous damage evolution, with linear and nonlinear laws of the parameter governing the rate of degradation. The CPD model provides a reasonable assessment of the experimental (monotonic) curve enveloping the hysteretic response when a high (constant) value of Ψ or variability with the current value of inelastic deformation are considered. An acceptable fit with the experimental cyclic response is partially guaranteed only during the unloading phases for an updating value of Ψ, in line with nonlinear degradation rules (ε<1).

Finally, the nonlinear seismic analysis of a SDOF system equivalent to a r.c. framed structure confirms that the main modes of cyclic deterioration (i.e. stiffness reduction during the unloading and reloading phases, strength decay related to pinching effects and cyclic and in-cycle degradations) and the capacity boundary curves are highly sensitive to the dynamic nature of the loading protocol and the deteriorating rules of the CPD model. This highlights the importance of accounting for the nonlinear cyclic response appropriately through an efficient and accurate numerical model, which also takes into account the fact that performance-based design procedures are frequently based on pushover curves that do not include information on the hysteretic behaviour of the structural system.

ACKNOWLEDGEMENTS

The present work was financed by Re.L.U.I.S. (Italian network of university laboratories of earthquake engineering), in accordance with the "Convenzione D.P.C.-Re.L.U.I.S. 2019-2021, WP15, Code Revisions for Isolation and Dissipation".

REFERENCES

Bouc, R., 1967. Forced vibration of mechanical systems with hysteresis. *Proceedings of the Fourth Conference on Nonlinear Oscillation*, Prague, Czechoslovakia.

Bozorgnia, Y., Bertero, V.V., 2003. Damage spectra: characteristics and applications to seismic risk reduction. *Journal of Structural Engineering (ASCE)*, **129**(10), 1330-1340.

Cosenza, E., Manfredi, G., Ramasco, R., 1993. The use of damage functionals in earthquake engineering: a comparison between different methods. *Earthquake Engineering and Structural Dynamics*, **22**, 855-868.

D.M., 1996. Norme tecniche per le costruzioni in zone sismiche e relative istruzioni. Italian Ministry of Public Works, D.M. 16-01-1996 and C.M. 10-04-1997.

Do, T.N., Filippou, F.C., 2018. A damage model for structures with degrading response. *Earthquake Engineering and Structural Dynamics*, **47**, 311-332.

FEMA P440A, 2009. Applied Technology Council. Effects of strength and stiffness degradation on seismic response. Technical Report, Washington, D.C., Federal Emergency Management Agency.

Ibarra, L.F., Medina, R.A., Krawinkler, H., 2005. Hysteretic models that incorporate strength and stiffness deterioration. *Earthquake Engineering and Structural Dynamics*, **34**(12), 1489-1511.

Kappos, A.J., 1997. Seismic damage indices for RC buildings: evaluation of concepts and procedures. *Progress in Structural Engineering and Materials*, **I**, 78-87.

Krätzig, W., Meyer, I., Meskouris, K., 1989. Damage evolution in reinforced concrete members under cyclic loading. In: Structural Safety and Reliability American Society of Civil Engineers: San Francisco, California, USA 1989; 795-804.

Luzi, L., Puglia, R., Russo, E., 2016. Engineering Strong Motion Database, version 1.0**.** Istituto Nazionale di Geofisica e Vulcanologia, Observatories & Research Facilities for European Seismology, 10.13127/ESM"

Mazza, F., 2018. Shear modelling of the beam-column joint in the nonlinear static analysis of r.c. framed structures retrofitted with damped braces. *Bulletin of Earthquake Engineering*, **6**, 2043-2066.

Mazza, F., 2019. A plastic-damage hysteretic model to reproduce strength stiffness degradation. *Bulletin of Earthquake Engineering*, **17**(6), 3517-3544.

Mazza, F., Mazza, M., 2010. Nonlinear analysis of spatial framed structures by a lumped plasticity model based on the Haar-Kàrmàn principle. *Computational Mechanics*, **45**(6), 647-664.

Mehanny, S., Deierlein, G., 2001. Seismic damage and collapse assessment of composite moment frames. *Journal of Structural Engineering (ASCE)*, **127**(9), 1045-1053.

N.T.C.18. Updating of the Technical Regulations for the Constructions. Italian Ministry of the Infrastructures, D.M. 17-01-2018.

Park, Y.J., Reinhorn, A.M., Kunnath, S.K., 1987. IDARC: Inelastic damage analysis of reinforced concrete frame-shear-wall structures. State University of New York at Buffalo, Technical Report, NCEER-87-0008.

Ruiz-Garcia, J., Miranda, E., 2005. Performance-based assessment of existing structures accounting for residual displacements. John A. Blume Earthquake Engineering Center, Department of Civil and Environmental Engineering, Stanford University, Stanford (California) Report No. 153.

Sezen, H., 2002. Seismic behavior and modeling of reinforced concrete building columns. PhD thesis, Dept. of Civil and Environmental Engineering, University of California at Berkeley, Berkeley, California.

Sivaselvan, M.V., Reinhorn, A.M., 2000. Hysteretic models for deteriorating inelastic structures. *Journal of Engineering Mechanics (ASCE)*, **126**(6), 633-640.

Song, J.K., Pincheira, J., 2000. Spectral displacement demands of stiffness-and strength-degrading systems. *Earthquake Spectra*, **16**(4), 817-851.

Takeda, T., Sozen, M.A., Nielsen, N.N., 1970. Reinforced concrete response to simulated earthquakes. *Journal of Structural Division (ASCE)*, **96**(12), 2557-2573.

Vaiana, N., Sessa, S., Marmo, F., Rosati, L., 2018. A class of uniaxial phenomenological models for simulating hysteretic phenomena in rate-independent mechanical systems and materials. *Nonlinear dynamics*, **93**(3), 1647-1669.

Vamvatsikos, D., Cornell, C.A., 2205. Direct estimation of seismic demand and capacity of multidegree-of-freedom systems through incremental dynamic analysis of single degree of freedom approximation. *Journal of Structural Engineering (ASCE)*, **131**(4), 589-599.

Wen, Y.-K., 1976. Method for random vibration of hysteretic systems. *Journal of Engineering Mechanics Division, ASCE*, **102**(2), 249-263.